Heliyon 10 (2024) e36454

Contents lists available at ScienceDirect

Heliyon

journal homepage: www.cell.com/heliyon

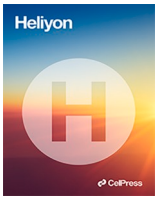

Research article

Experimental and numerical investigation of waterjet interaction with liver in connection with surgical technique

R. Derakhshan [a,*], M.T. Ahmadian [b]

[a] School of Mechanical Engineering, Sharif University of Technology, Tehran, Iran
[b] School of Mechanical Engineering, Sharif University of Technology, Center of Excellence in Design, Robotic and Automation, Tehran, Iran

ARTICLE INFO

Keywords:
SPH-FEM
VUSDFLD
Damage
Hyperelastic
Element deletion
Maximum principal strain

ABSTRACT

Hepatectomy, or liver resection, is a process by which through surgery part or all of the liver is removed. In this operation, less bleeding, negligible damage and fast removal are the most important requirements. Surgery through waterjet is one of the most efficient techniques which is widely used in hepatectomy. Some clinical studies are conducted to investigate waterjet method in liver resection. In the present study interaction of waterjet with liver during the process of the surgery is investigated in terms of mechanical engineering.

For this purpose, a system of waterjet is designed to consider the interaction of waterjet with liver at different nozzle diameter and velocities. For validation, SPH-FEM model is used to analyze waterjet interaction with hyperelastic liver. In this model, liver cutting is simulated using element deletion defined by a subroutine code based on maximum principal strain criterion. Depth of cut along with degraded volume are measured experimentally and compared with simulated method.

Results show that good agreement exists between experimental and simulation finding. By comparing depth of cut in the experimental and simulation results, it can be seen that liver behavior changes from brittle to ductile by increasing waterjet velocity during the experimental tests. For the simulation, maximum principal strain threshold is set to be between 0.1 and 0.4. However, the best agreement between experimental and simulation results exists at maximum principal strain threshold equal to 0.2. The findings can help surgeons to find the best working range of waterjet device and the most efficient operation.

1. Introduction

Hepatectomy or liver resection is a surgical operation for the removal of part or all of the liver. The body can handle the removal of up to two-thirds of the liver. Within 3 months of the surgery, the remainder of the liver will grow back to near-normal size [1]. When it comes to the resection of the liver, fast removal, minimal blood loss, and negligible tissue damage are the most important parameters in the operation [2,3]. Many interventions have been introduced in liver surgery to minimize the risk of postoperative complications caused by excessive bleeding [4]. Techniques such as vascular occlusion [5] and low central venous pressure anesthesia [6] are widely employed to minimize blood loss during hepatectomy. Various hemostatic devices, including the argon beam coagulator [7], ultrasonic coagulating shears [8], saline-linked radiofrequency technology [9,10], and vascular staplers [11], are implemented to control

* Corresponding author.
E-mail addresses: r.derakhshan94@sharif.edu, rzdrksn@gmail.com, rdaa@connect.ust.hk (R. Derakhshan), ahmadian@sharif.edu (M.T. Ahmadian).

https://doi.org/10.1016/j.heliyon.2024.e36454
Received 16 June 2023; Received in revised form 15 July 2024; Accepted 15 August 2024
Available online 18 August 2024
2405-8440/© 2024 The Authors. Published by Elsevier Ltd. This is an open access article under the CC BY-NC-ND license (http://creativecommons.org/licenses/by-nc-nd/4.0/).

bleeding during liver resection. The finger fracture method, developed in the 1960s [12], enables liver parenchymal division while preserving the integrity of hepatic vessels. Subsequently, the clamp crushing method [13], ultrasonic aspirators (UA) [14], and waterjet dissectors [15,16] were introduced. However, the optimal procedure for liver resection, which ensures preservation of hepatic vessels, minimal blood loss, and shorter procedure time, has not been specifically determined [17,18].

Studies demonstrate that the waterjet dissection technique offers swiftness, feasibility, oncological safety, and effectiveness in liver resection surgery, reducing bleeding [15,17,19,20]. In addition, due to its uncomplicated technique, waterjet applications are widely implemented, and its low cost facilitates its extensive use for economic reasons [20]. For instance, nowadays, efforts have been made to utilize waterjet for tumor removal to minimize operation risks [21]. Ogawa et al. recently conducted a study on a novel technique for removing hypophysis tumors in the skull base region. They applied the pulsed laser-induced liquid jet (LILJ) system, which efficiently and safely removes tumors without causing harm to blood vessels and nerves [22]. Furthermore, Nakagawa et al. published a study on the safety of using the LILJ system, concluding that waterjet is a safe method for removing lesions in the pituitary gland and its surrounding area [23]. Endo et al. used an actuator-driven pulsed waterjet for the resection of brain and spinal cord cavernous malformations [24]. Derakhshan et al. conducted an investigation into the interaction between a waterjet and the spinal cord, including various meningeal layers, to establish threshold characteristics for a safe surgical procedure. Ensuring the safety of waterjet characteristics is crucial to minimize treatment risks, particularly in proximity to vulnerable organs like the spinal cord and optic nerves. Furthermore, they explored the impact of waterjet fluid density on the failure criteria of spinal cord surgery. The findings indicate that dura mater, as stiffest layer of meninges, exhibits sufficient durability to safeguard the spinal cord against rupture at pressures up to 8 bar [25,26].

Accurate modeling of the liver necessitates a profound understanding of its mechanical characteristics. Many studies have explored the mechanical properties of the liver. Umale et al. conducted measurements of the mechanical properties of specific liver components, such as Glisson's capsule and hepatic veins [27]. Elvírez et al. examined the distribution of liver stiffness in Cuban adults without liver disease and its correlation with age. Liver stiffness values ranged from 2.2 to 6.3 kPa, and the reference range (95 % CI) for 110 subjects without known liver disease was 4.2–4.6 kPa, with a mean value of 4.4 [28]. Other studies by Roulot, Corpechot, and Sirli reported liver stiffness values ranging from 3.3 to 8.0 kPa, 2.5–6.9 kPa, and 2.3–8.8 kPa, respectively [29–31]. These studies, performed in healthy individuals, established mean normal liver stiffness values ranging from 4.8 to 5.4 kPa [32]. Also, hyper-elastic properties of the human liver using different models have proposed in various studies, such as the neo-Hookean model [33,34], Mooney-Rivlin model [35–38], reduced polynomial models [39], Bogen model [33], and Ogden model [40–44]. The investigation of liver's hyper-elastic behavior under impact using a polynomial model has been carried out by Shao [45] and Miller [46].

Understanding how to model soft body tissue damage is another essential requirement for this project. Many studies have been conducted to explore the biomechanisms of organ injury, with one commonly used criterion being the maximum principal strain. According to this definition, injury occurs when strain values surpass the threshold for injury. Shigeta et al. employed a finite element (FE) model to predict internal organ injury [47], while Shao et al. focused specifically on blunt liver injury resulting from impact on the abdomen without rib cage fractures [45]. In these studies, the maximum principal strain value was utilized to assess liver injury under high-speed blunt impact. Untaroiu et al. investigated the effect of tensile loading on liver injury and the corresponding maximum principal strain value. Different loading rates ranging from 0.01 s^{-1} to 10 s^{-1} were employed, and the results indicated that the failure threshold ranged from approximately 0.2 to 0.4, depending on the loading rate. Moreover, this threshold value decreased as the loading rate increased [43].

One of the primary challenges in conducting in-vitro experimental investigations is the increasingly limited availability of fresh human specimens. Moreover, obtaining such specimens in sufficient quantities becomes necessary to account for the wide scattering effect caused by biological variability [48]. To address this issue, animal specimens are frequently used. Specifically, the histological structure of the liver is found to be remarkably similar among humans, cows, sheep, and goats [49–51].

This study focuses on the design of a waterjet instrument to explore the interaction between the waterjet and sheep liver. The depth of cutting is measured after applying the waterjet using nozzles with different diameters (0.2, 0.4, and 0.5 mm). Additionally, the minimum velocity required to cut the liver is determined for each nozzle. Furthermore, a 3D finite element model is developed in ABAQUS to simulate the interaction between the waterjet and the liver within the fixture. A VUSDFLD subroutine code is incorporated into the main model to implement element deletion based on the maximum principal strain. The study investigates the effects of various waterjet parameters and liver failure criteria on the depth of waterjet cutting through both experimental methods and FEM analysis. It is worth mentioning that the damage threshold, depth of cut, degraded volume, and waterjet flow rate play a crucial role for surgeons as they determine the optimal operating range of the waterjet device, allowing for the most efficient procedures with minimal blood loss.

2. Material & methods

2.1. The waterjet apparatus

Fig. 1-I depicts a schematic representation of the waterjet apparatus, which incorporates nozzles of varying diameters (0.2, 0.3, 0.4, 0.5 mm) to achieve different waterjet caliber ranges. To ensure consistent water pressure throughout the experiment, a controller system has been devised. This system features a microcontroller programmed in C++ that governs a solenoid valve to regulate and maintain the water pressure. Additionally, a relay is employed as an actuator to adjust the air compressor and sustain the desired water pressure. Consequently, the waterjet output velocity remains steady and constant throughout the testing phase.

2.2. Waterjet velocity calibration

The speed of the waterjet can be determined using Bernoulli's law, neglecting any energy losses. Eq. (1) presents the pressure between point 1 and point 2.

$$\frac{1}{2}\rho {V_1}^2 + P_1 + \rho g h_1 = \frac{1}{2}\rho {V_2}^2 + P_2 + \rho g h_2 \quad (1)$$

Point 1 is located within the tank, while point 2 represents the exit of the waterjet. In this system h_1 and h_2 are almost at the same level and V_1, P_2 may be assumed to zero. So, Eq. (1) can be simplified as Eq. (2):

$$P_1 = \frac{1}{2}\rho {V_2}^2 \quad (2)$$

As anticipated, a significant amount of energy is expected to be lost at the micrometer nozzle. To examine the relationship between waterjet velocity and pressure, a calibration procedure was conducted, and the results are presented in Fig. 1-II. It is worth noting that, according to Eq. (2), the waterjet velocity should be consistent for all nozzles since the equation is independent of the nozzle's diameter. Fig. 1-III displays the volumetric flow rate (Q = V*A) of the waterjet in relation to the pressure for pure water. The relationship between waterjet velocity and pressure can be depicted through regression equations outlined in Table 1.

2.3. Experiments

The test is designed to explore the interaction between the waterjet and the liver. To facilitate this investigation, a fixture is created using SolidWorks and Cura applications, as depicted in Fig. 2-a. The fixture is then fabricated using a 3D printer, as shown in Fig. 2-b.

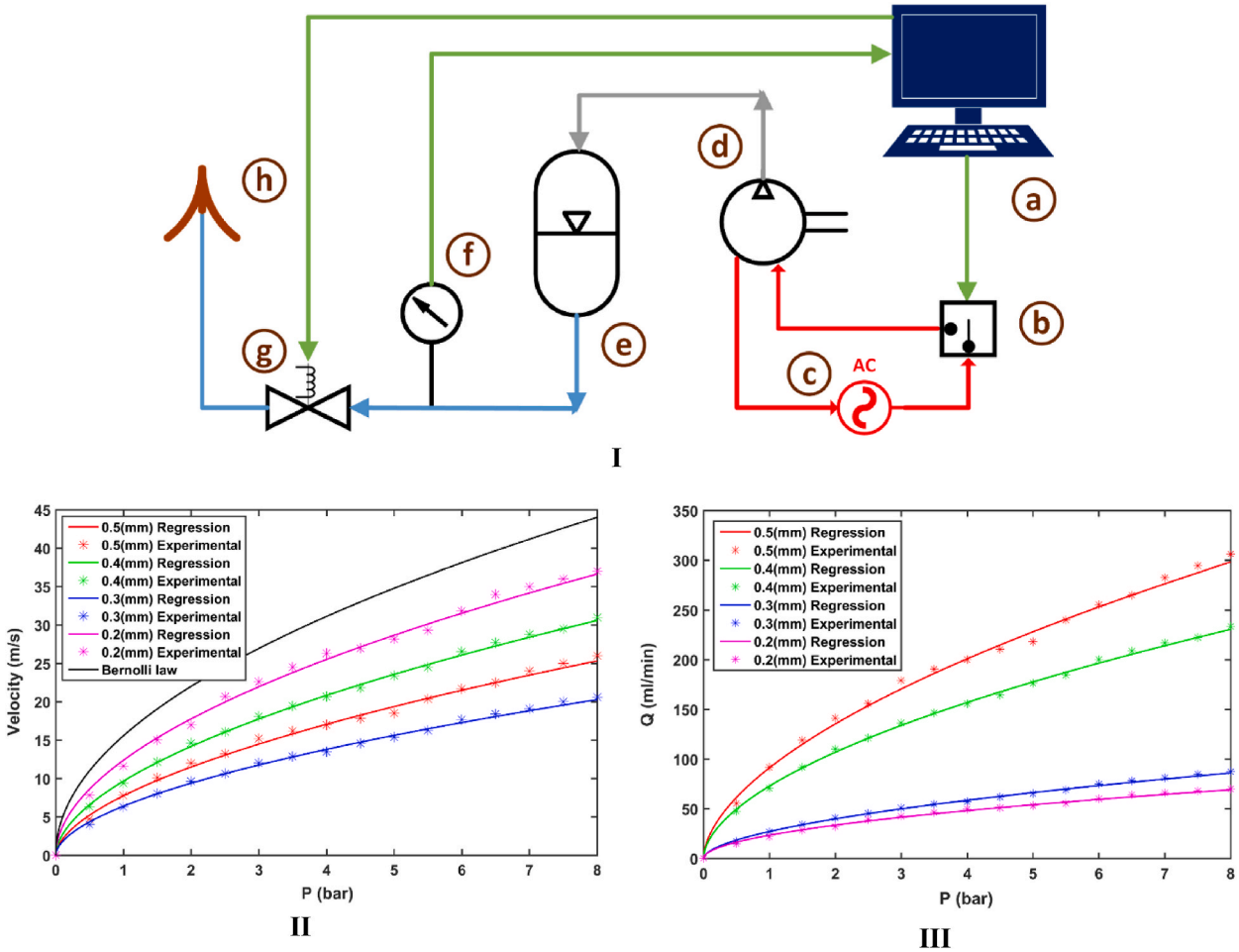

Fig. 1. I) Schematic of waterjet instrument; a) computer and microcontroller, b) relay coil, c) AC electrical power, d) air compressor, e) tank (pressure stabilizer) f) pressure gage, g) solenoid valve h) nozzle, green line: controlling signal, red line: electrical power line, grey line: air flow, blue line: water flow II) Waterjet velocity calibration on gage pressure III) Volumetric flow rate of waterjet versus pressure.

Table 1
Regression equations of waterjet velocity on gage pressure.

Nozzle caliber (mm)	Regression equation, $P(bar), \rho(kg/m^3), V(m/s)$	Standard Deviation (m/s)
Bernoulli's law	$V = \left(\frac{2*P*10^5}{\rho}\right)^{0.5}$	—
0.2	$V = \left(\frac{2*0.617728*P*10^5}{1000}\right)^{0.522187}$	0.664
0.3	$V = \left(\frac{2*0.139944*P*10^5}{1000}\right)^{0.556161}$	0.255
0.4	$V = \left(\frac{2*0.297553*P*10^5}{1000}\right)^{0.554777}$	0.302
0.5	$V = \left(\frac{2*0.181032*P*10^5}{1000}\right)^{0.570084}$	0.442

During the experiment, the waterjet is injected into the embedded liver within the sphere through a small hole (4 mm in diameter) located on the top. The resulting cutting depth and damage area of the liver are measured. The design of the fixture and the waterjet interaction are modeled after the operating principles employed by surgeons.

Samples are obtained from fresh sheep livers of the same race, male gender, with an average weight of approximately 47 ± 2 kg and an age of 2 years. Each experiment is conducted using three different nozzles: 0.2, 0.4, and 0.5 mm. To enhance reliability, each case is repeated five times. The nozzles are positioned 1 cm away from the prepared samples in order to prevent waterjet splash, as depicted in Fig. 2-a. The tests are carried out immediately after the samples are prepared to minimize any alterations in the liver properties. To measure the depth of the cutting, a liquid ink is added to the water tank (one percent in volume). Sufficient time (5 s) is allotted for each test to ensure that the cutting depth reaches a stable state, although this is typically achieved in less than a second.

2.4. Finite element modeling

2.4.1. Part and property

A 3D finite element model is developed in ABAQUS to simulate the interaction between the waterjet and the liver within the fixture. The model consists of three distinct parts is illustrated in Fig. 3: the liver (Fig. 3-a), the fixture (Fig. 3-b) and the waterjet (Fig. 3-c). The fixture is treated as a thin rigid spherical structure with an inner diameter of 10 mm and a hole on the top. The liver is encapsulated within the fixture. The mechanical properties of the liver are outlined in Table 2.

The waterjet part in the model represents a long, thin, cylindrical 3D deformable structure, with the thickness determined by the nozzle inlet diameter. The physical properties of water utilized in the simulation are provided in Table 3.

2.4.2. Mesh

Due to the limitation of ABAQUS in analyzing large deflection of fluid materials using finite element method (FEM), an alternative approach is employed for the waterjet part known as the Smoothed Particle Hydrodynamics (SPH) method. In this method, the waterjet part is initially meshed using C3D8R type elements and Hex-structured shapes. Subsequently, the mesh is converted into particles. The approximate global size of the meshes is around 0.08 mm. To facilitate the analysis, the waterjet part is partitioned into four sections from the cross-section.

The liver part is meshed using C3D8R Hex-structured shape elements with an approximate global size of 0.1 mm. For this part, the option of element deletion should be selected. To obtain higher quality meshes, the spherical portion of the liver is divided into eight symmetrical parts. Despite being a rigid component, the fixture needs to be meshed in ABAQUS like the other parts. It is advisable to use finer meshes for the fixture compared to those used for the liver.

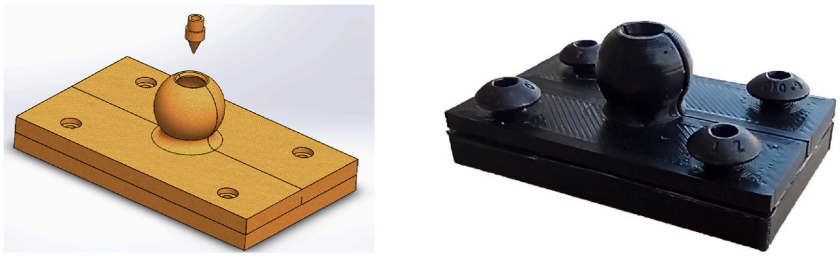

a **b**

Fig. 2. a) designed file for fixture in SolidWorks and Cura, b) built fixture by 3D printer.

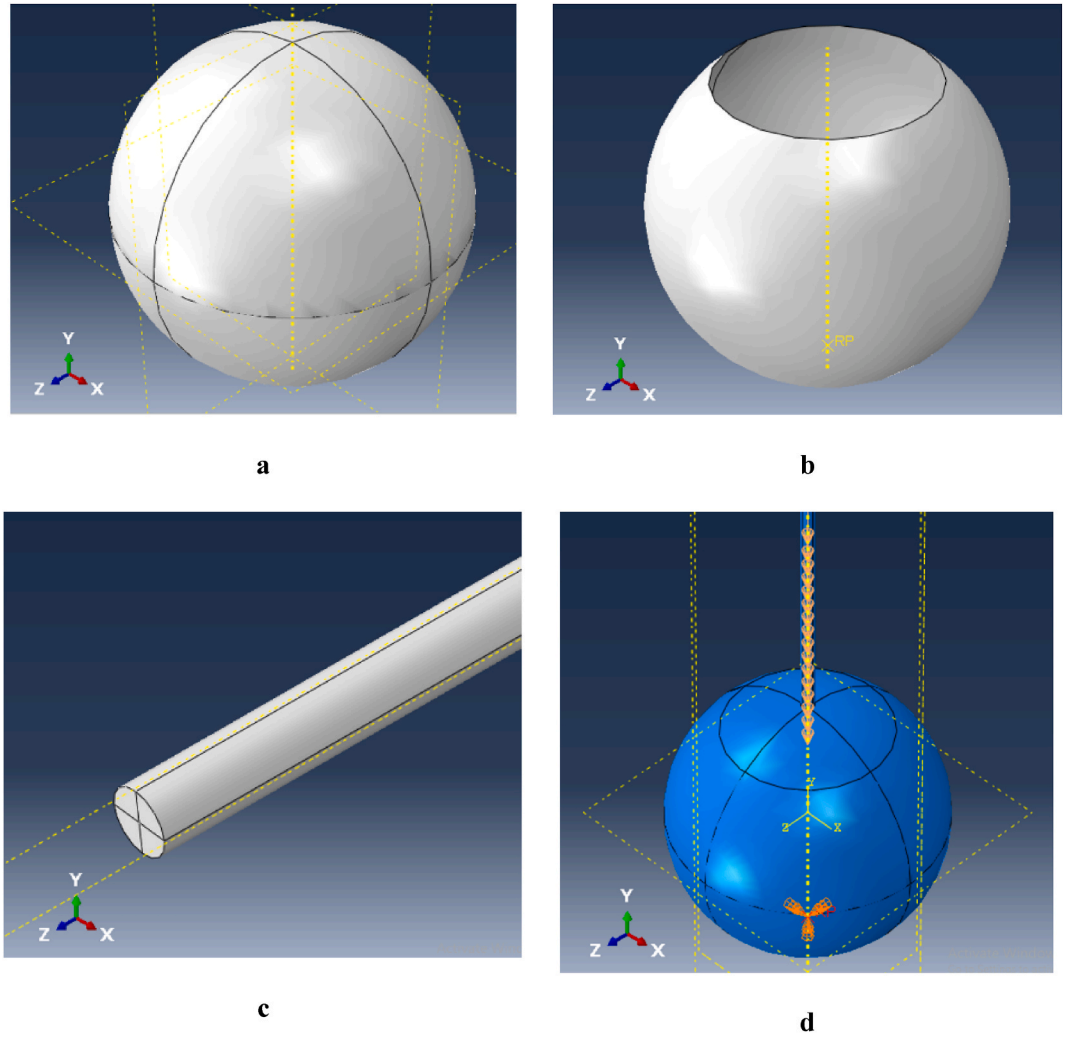

Fig. 3. Three parts of model: a) Liver, b) Fixture and c) Waterjet and d) Initial and boundary conditions of model.

Table 2
Mechanical properties of the liver part used in FEM model [43].

Type	3D, Deformable, Homogenous, solid
Density (uniform distribution)	**1.1** g/cm^3
Hyper-elastic (polynomial order 2)	**C10 = C01 = 6206 Pa;** **C20 = C02 = 3492 Pa;** **C11 = 0;** **D1 = D2 = 0;**

Table 3
Physical properties of waterjet part used in FEM model.

Type	3D, Deformable, Homogenous, solid
Density (uniform distribution)	**1** g/cm^3
Viscosity (at 20 C^o**)**	**1 mPa**

2.4.3. Step

A dynamic explicit step is defined to investigate interaction behavior after initial step. In this step, Nlgeom (geometric nonlinearity) should be turned on because there is large deflection and magnitude of the displacements affects the response of the structure.

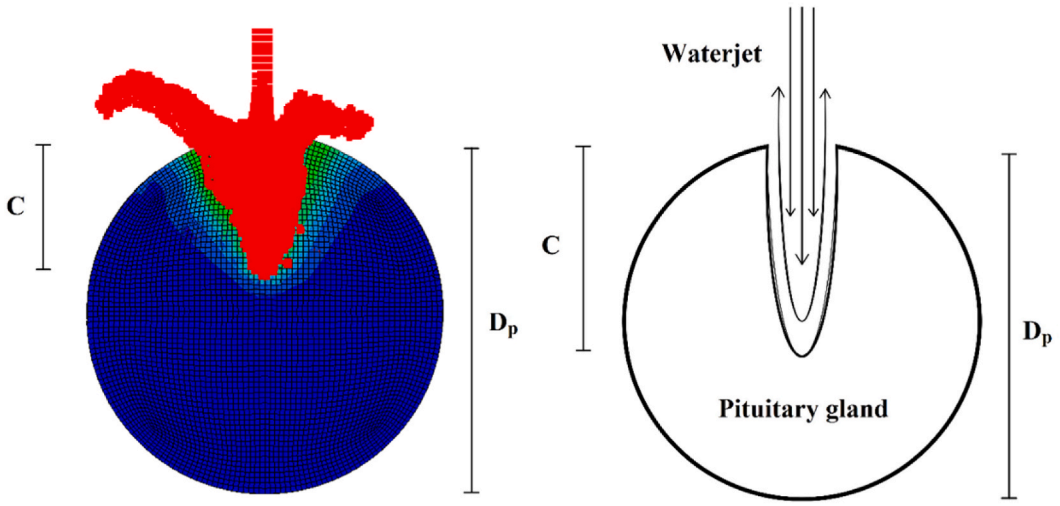

a

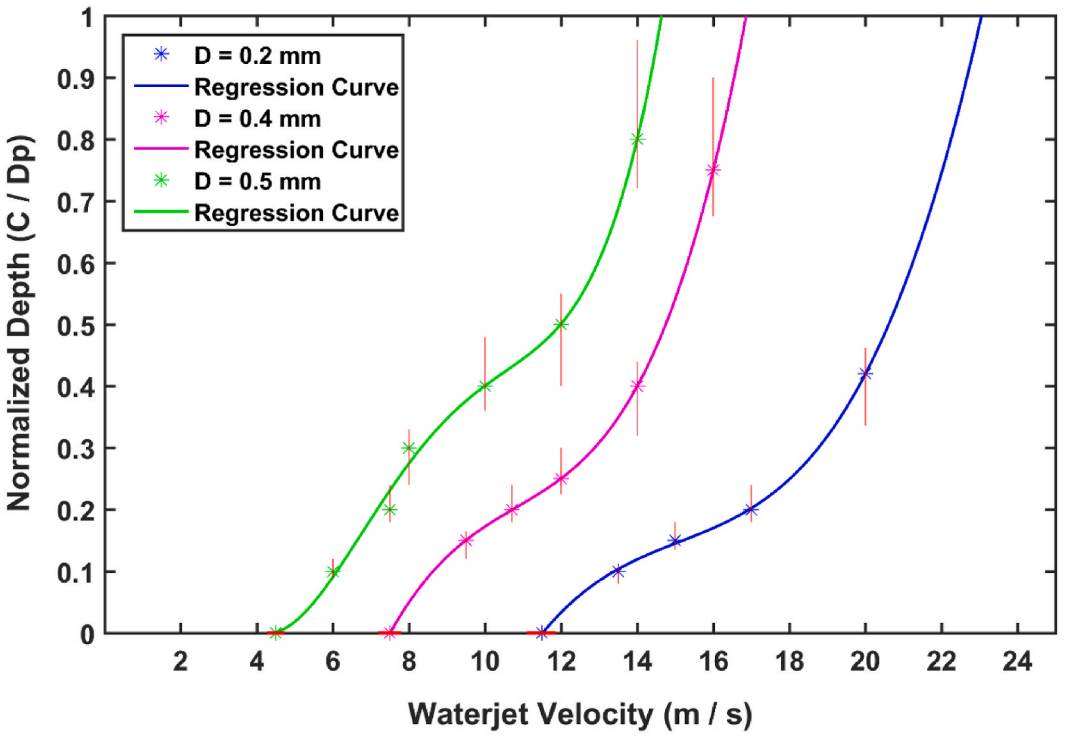

b

Fig. 4. a) Waterjet cutting parameters in cross section of FEM model, b) Normalized depth of waterjet pierce for experimental tests.

2.4.4. Interaction

An interaction is defined in dynamic explicit step between all parts surface. With this definition, waterjet nodes, liver elements and fixture elements have interaction with each other during the simulation. All contacts and interactions are defined as frictionless.

2.4.5. Load

Initial velocity of waterjet nodes is applied in Initial step and computed in Dynamic step. Also, in boundary conditions, fixture pert could be fixed in all rotational and translational motions. This boundary condition is created in initial step and propagated to Dynamic step (Fig. 3-d).

2.4.6. Job

ABAQUS software is unable to delete the elements with a certain stress or principal strain by default. This limitation can potentially be overcome by implementing appropriate subroutine codes. A VUSDFLD code is written based on maximum 3D principal strain and applied to the model in the job module. Subroutines are commonly written in FORTRAN, often using Intel Fortran as the programming language. Intel Fortran Compiler works under Microsoft Visual Studio. Consequently, ABAQUS, Intel Fortran and Microsoft Visual Studio must be compatible and linked to one another. A counter is included in the subroutine code to print the number of eliminated elements and their ID in the output text file. It is important to highlight that simulating this model is a computationally intensive task that requires significant CPU resources and time. Typically, each simulation run takes more than 24 h when employing parallelization mode with 8 processors distributed across 8 domains, utilizing approximately 90 percent of the CPU performance.

2.5. Ethics statement

All the tests conducted in this study utilized livers that were obtained from sheep carcasses, and no procedures were performed on human bodies. Also, no anesthesia, euthanasia, or any form of animal sacrifice was involved in this study.

3. Results and discussion

Fig. 4-a represents schematic diagram of liver sample cross section during waterjet cutting. In this figure Dp is liver diameter (10 mm) and C is the depth of waterjet cutting. Fig. 4-b shows the experimental normalized depth of waterjet cut (C/Dp) versus waterjet velocity with pressure up to 2.5 bar.

To observe the trend of normalized depth versus waterjet velocity, a polynomial regression curve is fitted based on experimental findings for different nozzle diameter. In this figure, curve fitting is based on mean values of normalized depth. While red vertical bars represent the scattering of data around the mean values.

The minimum jet velocity required to penetrate the liver may be defined as V_di. The velocity needed to achieve a waterjet cutting depth equal to the entire sample thickness is defined as V_da. The values of V_di and V_da depend on liquid density and nozzle diameter. The experimental values of V_di and V_da for different nozzles are presented in Fig. 4-b and Table 4. The scatter data of V_di around the mean value is shown by horizontal red bars on the x-axis of Fig. 4-b.

V_di and V_da decrease as nozzle diameter increases. For the same waterjet velocity, cutting depth increases with increasing nozzle diameter.

In finite element method, the maximum principal strain required for failure of the elements briefly indicated by MPS. This value varies from 0.2 to 0.4 for liver depending on loading rate [43]. Fig. 5-II shows experimental and simulated normalized depth of cut versus velocity for nozzle of 0.4 mm in diameter with different MPS. As shown, as the MPS increases from 0.1 to 0.4, the cutting depth decreases for the same waterjet velocity, while the V_di and V_da values increase.

In waterjet interaction with substrate (liver), two parameters are of importance in cutting. The first parameter is the impact of waterjet with the substrate in which the rupture takes place in elements close to surface and in early moments of interaction (Fig. 5-IV-a). Then with the penetration of waterjet into the greater depth, the stress applied by the waterjet on the elements causes the rupture of the tissue (Fig. 5-IV-b).

In other words, when the waterjet velocity is near to V_di, the first parameter is the primary factor influencing the cutting process. This is because, at velocities close to V_di, the waterjet can only pierce facial elements, resulting in a high loading rate upon impact. Consequently, given the high loading rate, it is anticipated that MPS would approach its minimum value for the liver (0.2). This observation indicates that, under these conditions, the substrate exhibits behavior characteristic of a brittle material. It is well-established that rupture occurs in brittle materials at lower strain levels.

As the velocity increases, the waterjet can penetrate deeper elements, making the second factor more influential. In this scenario, with an increase in cutting depth, the presence of fluid viscosity diminishes the waterjet's penetration. Consequently, the strain rate of

Table 4
Experimental values of V_di and V_da for different nozzles and their flow rates.

Nozzle Caliber (mm)	V_di (m/s)	Q (ml/s)	V_da (m/s)	Q (ml/s)
0.2	**11.3**	**0.42**	**23**	**0.86**
0.4	**7.7**	**0.95**	**16.8**	**2.13**
0.5	**4.5**	**0.84**	**14.6**	**2.72**

internal elements decreases. It is expected that MPS would approach its maximum value for the liver (0.4), indicating a ductile material behavior in the substrate.

Indeed, it may be claimed that for velocities close to V_di, the substrate behaves as a brittle material, while as the velocity increases, it tends to a ductile material. This statement is observable in the comparison of experimental and FEM results in Fig. 5. With an increase in waterjet velocity, the curves related to the experimental results in Fig. 5-I, Fig. 5-II and Fig. 5-III tend to shift from the MPS = 0.2 curve towards the MPS = 0.4 curve. Fig. 5-I and Fig. 5-III also present normalized depth of waterjet cutting for nozzle diameter of 0.2 and 0.5 mm at different velocities.

In liver resection with waterjet, the removal of injected liquid and blood is accomplished using a suction tool. The flow and debris removal within the surgical area are critical parameters in waterjet surgery. The volumetric flow rates of the waterjet at V_di and V_da for various nozzle sizes are outlined in Table 4. Notably, the minimum flow rate is observed for a nozzle diameter of 0.2 mm. This implies that for a successful surgery with the least flow rate, a nozzle with a diameter of 0.2 mm would be an appropriate choice.

Fig. 6-a shows normalized depth of cut obtained using FEM for different nozzles with MPS = 0.3.

In addition to considering the depth of the cut, further investigation of the degraded volume could provide a better understanding of the situation. The subroutine code has the capability to count the number of deleted elements and record their IDs in a text file. At the end of each iteration of the simulation, the code calls for the calculation of strain matrix and other requested outputs. 3D principal strains are then calculated. If the maximum principal strain of each element exceeds a certain threshold (referred to as MPS), the element is deleted in that particular iteration. This process continues until the simulation is completed.

Fig. 6-b shows qualitative diagram of the normalized degraded volume in terms of waterjet velocity for different nozzles and MPS = 0.3. Normalized degraded volume may be defined as ratio of the number of deleted elements (Nd) to the total number of pituitary part elements (Nt). Fig. 6-c represents Fig. 6-b in logarithmic scale for vertical axis.

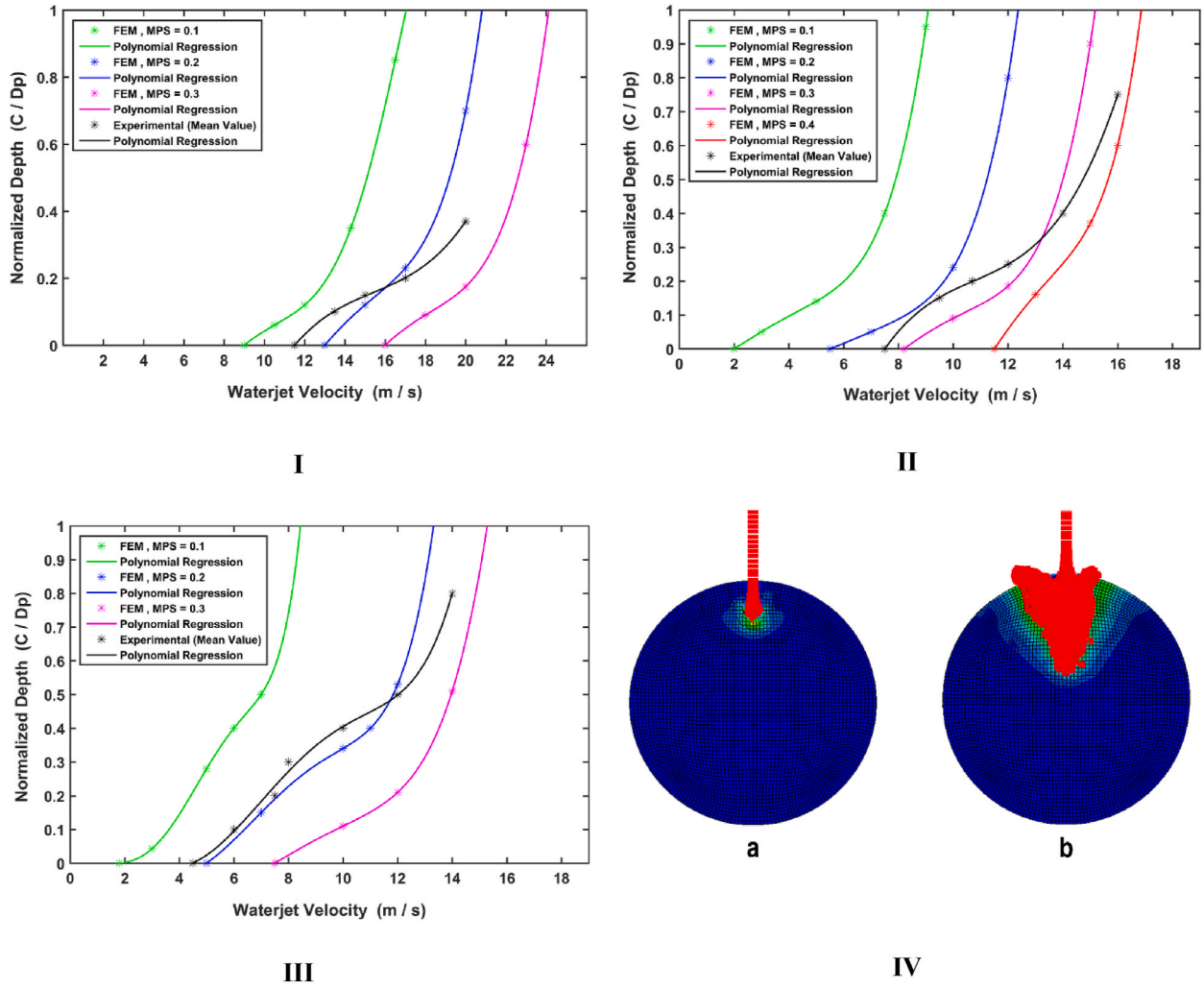

Fig. 5. Normalized depth of cut versus velocity for nozzle I) 0.2 mm, II) 0.4 mm, III) 0.5 mm, IV) schematic view from two factors of waterjet cutting.

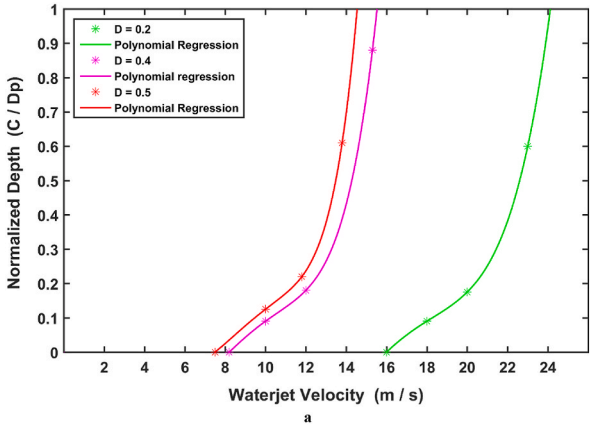

a

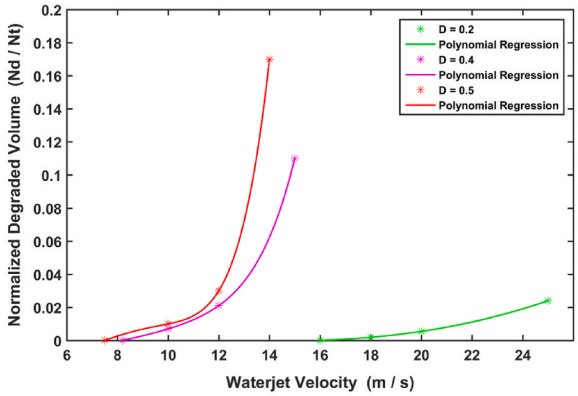

b

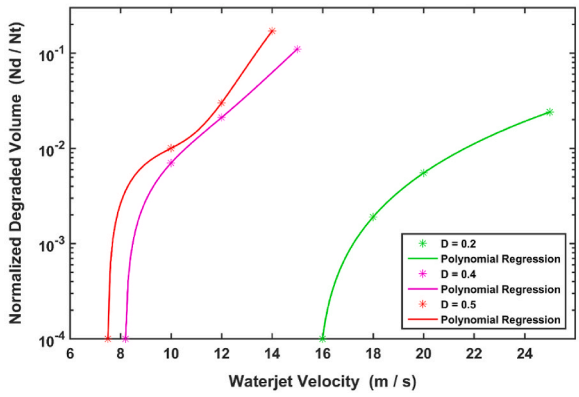

c

Fig. 6. a) Normalized depth of cut and b, c) Normalized degraded volume in terms of waterjet velocity for different nozzles and MPS = 0.3.

As shown in Fig. 6-a, there is no significant difference between depth of cut versus waterjet velocity for nozzles 0.4 and 0.5 mm. Whereas Fig. 6-b indicates degraded volume for nozzle with diameter of 0.5 mm is more than nozzle with diameter of 0.4 mm.

4. Conclusion

With the increasing use of waterjet in today's world, this method has found many applications in medicine. One of these applications is resection of liver. In this work, interaction of waterjet with pituitary gland is studied. For this purpose, a waterjet setup is designed to investigate effects of different parameters of waterjet on cutting depth and degraded volume. Also, a 3D finite element model is employed to compare simulation and experiment results. A VUSDFLD subroutine code is imported into FEM model to define

element deletion based upon maximum principal strain.

The results indicate that, for a given waterjet velocity, the depth of cut increases as the nozzle diameter increases, while V_di and V_da values decrease with increasing nozzle diameter. Additionally, the simulation findings reveal that by increasing the MPS from 0.1 to 0.4, the cutting depth decreases at a constant waterjet velocity, while the V_di and V_da values increase.

The cutting of the liver is influenced by two parameters. The first, due to impact that has major role in early moment of interaction and applied to elements in close proximity to the surface. The second, in the following, as a consequence of stress applied by waterjet on deeper elements. In other words, for waterjet velocities close to V_di, the first parameter becomes more significant, leading to the liver behaving like a brittle material. However, as the waterjet velocity increases, the second factor assumes a more important role, causing the liver to exhibit characteristics of a ductile material. This observation can also be confirmed by comparing the depth of cut in experimental and simulation results, as the velocity of waterjet increases, experimental results tend to larger MPS.

By considering volumetric flow rate in waterjet technique, results advise that nozzle with 0.2 mm is suitable choice to have successful surgery with minimum flow rate. In addition to analyzing the depth of cut, investigating the degraded volume is important and can provide valuable insights for a better understanding of the cutting process. The degraded volume for the nozzle with a diameter of 0.5 mm is greater than that of the nozzle with a diameter of 0.4 mm, despite there being no significant difference in the depth of cut versus waterjet velocity for these nozzles.

CRediT authorship contribution statement

R. Derakhshan: Writing – review & editing, Writing – original draft, Visualization, Validation, Software, Resources, Project administration, Methodology, Investigation, Funding acquisition, Formal analysis, Data curation, Conceptualization. **M.T. Ahmadian:** Writing – review & editing, Supervision.

Declaration of competing interest

The authors declare that they have no known competing financial interests or personal relationships that could have appeared to influence the work reported in this paper.

Appendix A. Supplementary data

Supplementary data to this article can be found online at https://doi.org/10.1016/j.heliyon.2024.e36454.

References

[1] S. Wilner, M. Silva, A. Soonawalla, About Liver Resection, Oxford University Hospitals NHS Trust, 2022.
[2] Alessandro Michele Bonomi, Alessia Kersik, Greta Bracchetti, Christian Cotsoglou, 3D reconstruction in complex parenchymal sparing liver surgery, Heliyon 9 (3) (2023) e13857, https://doi.org/10.1016/j.heliyon.2023.e13857. ISSN 2405-8440.
[3] C. Kotan, N.Y. Bayramov, T.M. Rzaev, A. Taş, U. Abbasov, Diameter and pressure of the water-jet for liver resection, E. J. Med. 6 (2) (2001) 43–47.
[4] W.R. Jarnagin, M. Gonen, Y. Fong, R.P. DeMatteo, L. Ben-Porat, S. Little, et al., Improvement in perioperative outcome after hepatic resection: analysis of 1,803 consecutive cases over the past decade, Ann. Surg. 236 (2002) 397–406 (discussion 406–7).
[5] J. Belghiti, R. Noun, E. Zante, T. Ballet, A. Sauvanet, Portal triad clamping or hepatic vascular exclusion for major liver resection: a controlled study, Ann. Surg. 224 (1996) 155–161.
[6] H. Chen, N.B. Merchant, M.S. Didolkar, Hepatic resection using intermittent vascular inflow occlusion and low central venous pressure anesthesia improves morbidity and mortality, J. Gastrointest. Surg. 4 (2000) 162–167.
[7] R.R. Postema, P.W. Plaisier, F.J. ten Kate, O.T. Terpstra, Haemostasis after partial hepatectomy using argon beam coagulation, Br. J. Surg. 80 (1993) 1563–1565.
[8] N. Kokudo, H. Kimura, H. Yamamoto, M. Seki, H. Ohta, T. Matsubara, et al., Hepatic parenchymal transection using ultrasonic coagulating shears: a preliminary report, J Hepatobiliary Pancreat Surg 7 (2000) 295–298.
[9] J. Arita, K. Hasegawa, N. Kokudo, K. Sano, Y. Sugawara, M. Makuuchi, Randomized clinical trial of the effect of a salinelinked radiofrequency coagulator on blood loss during hepatic resection, Br. J. Surg. 92 (2005) 954–959.
[10] R.T. Poon, S.T. Fan, J. Wong, Liver resection using a saline-linked radiofrequency dissecting sealer for transection of the liver, J. Am. Coll. Surg. 200 (2005) 308–313.
[11] P. Schemmer, H. Friess, C. Dervenis, J. Schmidt, J. Weitz, W. Uhl, et al., The use of endo-GIA vascular staplers in liver surgery and their potential benefit: a review, Dig. Surg. 24 (2007) 300–305.
[12] T.Y. Lin, K.M. Chen, T.K. Liu, Total right hepatic lobectomy for primary hepatoma, Surgery 48 (1960) 1048–1060.
[13] H. Bismuth, D. Houssin, D. Castaing, Major and minor segmentectomies "réglées" in liver surgery, World J. Surg. 6 (1982) 10–24.
[14] W.J. Hodgson, J. Morgan, D. Byrne, L.R. DelGuercio, Hepatic resections for primary and metastatic tumors using the ultrasonic surgical dissector, Am. J. Surg. 163 (1992) 246–250.
[15] H.G. Rau, A.P. Duessel, S. Wurzbacher, The use of water-jet dissection in open and laparoscopic liver resection, HPB (Oxford) 10 (2008) 275–280.
[16] C.M. Vollmer, E. Dixon, A. Sahajpal, M.S. Cattral, D.R. Grant, S. Gallinger, et al., Water-jet dissection for parenchymal division during hepatectomy, HPB (Oxford) 8 (2006) 377–385.
[17] C. Nakanishi, T. Nakano, A. Nakagawa, C. Sato, M. Yamada, N. Kawagishi, T. Tominaga, N. Ohuchi, Evaluation of a newly developed piezo actuator-driven pulsed water jet system for liver resection in a surviving swine animal model, Biomed. Eng. Online 15 (1) (2016 Jan) 1, 0.
[18] Y. Otsuka, H. Kaneko, S.P. Cleary, J.F. Buell, X. Cai, G. Wakabayashi, What is the best technique in parenchymal transection in laparoscopic liver resection? Comprehensive review for the clinical question on the 2nd International Consensus Conference on Laparoscopic Liver Resection, J. Hepato-Biliary-Pancreatic Sci. 22 (5) (2015 May) 363–370.
[19] D.N. Papachristou, R. Barters, Resection of the liver with a water jet, Br. J. Surg. 69 (2) (1982 Feb) 93–94.

[20] Y. Une, J. Uchino, T. Horie, Y. Sato, K. Ogasawara, A. Kakita, F. Sano, Liver resection using a water jet, Cancer Chemother. Pharmacol. 23 (1) (1989 Jan) S74–S77.
[21] A.H. Alamoud, E. Baillot, C. Belabbas, H. Samimi Ardestani, H. Bahai, A. Baldit, et al., Continuous and pulsed experiments with numerical simulation to dissect pituitary gland tumour by using liquid jet, Eng. Lett. 25 (3) (2017) 348–353.
[22] Y. Ogawa, A. Nakagawa, K. Takayama, T. Tominaga, Pulsed laser-induced liquid jet for skull base tumor removal with vascular preservation through the transsphenoidal approach: a clinical investigation, Acta Neurochir. 153 (4) (2011) 823–830, https://doi.org/10.1007/s00701-010-0925-x.
[23] A. Nakagawa, Pulsed laser-induced liquid jet system for treatment of sellar and parasellar tumors: safety evaluation, J. Neurol. Surg. Cent. Eur. Neurosurg. 76 (6) (2015) 473–482, https://doi.org/10.1055/s-0034-1396436.
[24] T. Endo, Y. Takahashi, A. Nakagawa, K. Niizuma, M. Fujimura, T. Tominaga, Use of actuator-driven pulsed water jet in brain and spinal cord cavernous malformations resection, Operative Neurosurgery 11 (3) (2015) 394–403, https://doi.org/10.1227/NEU.0000000000000867.
[25] R. Derakhshan, M.T. Ahmadian, M. Chizari, et al., Trimming of sheep spinal cord by waterjet; an experimental study, Heliyon 9 (7) (2023) e17872, https://doi.org/10.1016/j.heliyon.2023.e17872.
[26] R. Derakhshan, M.T. Ahmadian, Effect of sudden pressure on spinal cord and break down (dura mater, arachnoid mater and Pia mater) an experimental analysis on threshold levels, Sci. Iran. (2023). https://doi.org/10.24200/sci.2023.60335.6743.
[27] S. Umale, S. Chatelin, N. Bourdet, C. Deck, M. Diana, P. Dhumane, L. Soler, J. Marescaux, R. Willinger, Experimental in vitro mechanical characterization of porcine Glisson's capsule and hepatic veins, J. Biomech. 44 (9) (2011) 1678–1683, https://doi.org/10.1016/j.jbiomech.2011.03.029.
[28] Á. Elvírez-Gutiérrez, M.I. Castellanos-Fernández, W. Santillán-López, Z. Dorta-Guridi, E. Galbán-García, E. Arús-Soler, Liver stiffness reference values for healthy Cuban adults, International Journal of Cuban Health & Medicine 20 (1) (2018) 24–28, https://doi.org/10.37757/MR2018.V20.N1.6.
[29] D. Roulot, S. Czernichow, H. Le Clesiau, et al., Liver stiffness valued in apparently healthy subjects: influence of gender and metabolic syndrome, J. Hepatol. 4 (2008) 606–613.
[30] C. Corpechot, A. El Naggar, R. Poupon, Gender and Liver: is the liver stiffness weaker in weaker sex? Hepatology 44 (2006) 513–514.
[31] R. Sirli, I. Sporea, A. Tudora, et al., Transient elastographic evaluation of subjects without known hepatic pathology: does age change the liver stiffness? J Gastrointest Liver Dis. 18 (2009) 57–60.
[32] S. Colombo, L. Belloli, M. Zaccanelli, E. Badia, C. Jamoletti, M. Buonocore, P.D. Poggio, Normal liver stiffness and its determinants in healthy blood donors, Dig. Liver Dis. 43 (3) (2011) 231–236, https://doi.org/10.1016/j.dld.2010.07.008.
[33] C. Chui, E. Kobayashi, X. Chen, T. Hisada, I. Sakuma, Combined compression and elongation experiments and non-linear modelling of liver tissue for surgical simulation, Med. Biol. Eng. Comput. 42 (6) (2004) 787–798.
[34] B. Ahn, J. Kim, Measurement and characterization of soft tissue behavior with surface deformation and force response under large deformations, Med. Image Anal. 14 (2) (2010) 138–148.
[35] T. Hu, J.P. Desai, A biomechanical model of the liver for reality-based haptic feedback, in: Medical Image Computing and Computer-Assisted Intervention-MICCAI, Springer, Berlin/Heidelberg, 2003, pp. 75–82, https://doi.org/10.1007/978-3-540-39899-8_10.
[36] S. Umale, C. Deck, N. Bourdet, P. Dhumane, L. Soler, J. Marescaux, R. Willinger, Experimental mechanical characterization of abdominal organs: liver, kidney & spleen, J. Mech. Behav. Biomed. Mater. 17 (2013) 22–33.
[37] Y. Fu, C. Chui, C. Teo, Liver tissue characterization from uniaxial stress–strain data using probabilistic and inverse finite element methods, J. Mech. Behav. Biomed. Mater. 20 (2013) 105–112.
[38] Y. Fu, C. Chui, Modelling and simulation of porcine liver tissue indentation using finite element method and uniaxial stress–strain data, J. Biomech. 47 (10) (2014) 2430–2435.
[39] K. Lister, Z. Gao, J.P. Desai, Development of in vivo constitutive models for liver: application to surgical simulation, Ann. Biomed. Eng. 39 (3) (2011) 1060–1073.
[40] Hu T, Desai J P, Characterization of soft-tissue material properties: large deformation analysis. In Medical Simulation. 2004; pages 28–37. Springer, Berlin/Heidelberg.
[41] Z. Gao, J.P. Desai, Estimating zero-strain states of very soft tissue under gravity loading using digital image correlation, Med. Image Anal. 14 (2) (2010) 126–137.
[42] C.D. Untaroiu, Y.C. Lu, Material characterization of liver parenchyma using specimen-specific finite element models, J. Mech. Behav. Biomed. Mater. 26 (2013) 11–22.
[43] C.D. Untaroiu, Y.C. Lu, S.K. Siripurapu, A.R. Kemper, Modeling the biomechanical and injury response of human liver parenchyma under tensile loading, J. Mech. Behav. Biomed. Mater. 41 (2015) 280–291, https://doi.org/10.1016/j.jmbbm.2014.07.006.
[44] Y.C. Lu, A.R. Kemper, C.D. Untaroiu, Effect of storage on tensile material properties of bovine liver, J. Mech. Behav. Biomed. Mater. 29 (2014) 339–349.
[45] Y. Shao, D. Zou, Z. Li, L. Wan, Z. Qin, et al., Blunt liver injury with Intact ribs under impacts on the abdomen: a biomechanical investigation, PLoS One 8 (1) (2013) e52366, https://doi.org/10.1371/journal.pone.0052366.
[46] K. Miller, Constitutive modelling of abdominal organs, J. Biomech. 33 (3) (2000) 367–373.
[47] K. Shigeta, Y. Kitagawa, T. Yasuki, Development of Next Generation Human FE Model Capable of Organ Injury Prediction, U. S. Department of Transportation, 2009, 1200 New Jersey Avenue SE Washington DC 20590 USA.
[48] R.B. Ashman, J.E. Bechtold, W.T. Edwards, C.E. Johnston, P.C. McAfee, A.F. Tencer, In vitro spinal arthrodesis implant mechanical testing protocols, J. Spinal Disord. 2 (4) (1989) 274–281.
[49] K.E. Madhan, S. Raju, Comparative histology of human and cow, goat and sheep liver, J. Surg. Acad. 4 (1) (2014) 10–13.
[50] M. Shri, H. Agrawal, P. Rani, D. Singh, S.K. Onteru, Hanging Drop, A best three dimensional (3D) culture method for primary Buffalo and sheep hepatocytes, Sci. Rep. 7 (1) (2017) 1203, https://doi.org/10.1038/s41598-017-01355-6.
[51] Philipp Felgendreff, Claudia Schindler, Franziska Mussbach, Chichi Xie, Felix Gremse, Utz Settmacher, Uta Dahmen, Identification of tissue sections from decellularized liver scaffolds for repopulation experiments, Heliyon 7 (2) (2021) e06129, https://doi.org/10.1016/j.heliyon.2021.e06129. ISSN 2405-8440.